


## High-contrast interaction-free quantum imaging method

Sepideh Ahmadi<sup>1,2</sup>, Erhan Saglamyurek<sup>2,3</sup>, Shabir Barzanjeh<sup>2,3,\*</sup> and Vahid Salari<sup>2,3,†</sup>

<sup>1</sup>*Department of Physics, Isfahan University of Technology, Isfahan 8415683111, Iran*

<sup>2</sup>*Department of Physics and Astronomy, University of Calgary, Calgary T2N 1N4, Alberta, Canada*

<sup>3</sup>*Institute for Quantum Science and Technology, University of Calgary, Calgary T2N 1N4, Alberta, Canada*

 (Received 27 July 2022; revised 6 February 2023; accepted 24 February 2023; published 17 March 2023)

Quantum imaging techniques offer enhanced resolution, contrast, and precision at ultralow illumination levels compared to traditional imaging approaches. Relying on the unique properties of entangled photon pairs, two of these techniques stand out: the correlation-based quantum imaging technique provides visibility enhancement in imaging of a low-reflectivity object which is subject to excessive noise and losses, while the interaction-free ghost imaging allows for probing the presence of an object with an ultimately low number of photons. Here we propose a quantum imaging scheme that combines the unique advantages of these two approaches. We show that this scheme offers high-contrast imaging of objects with a minimal number of photons that can minimize thermal noise efficiently and create background-free images. We anticipate that this approach can find application in the imaging of photosensitive biological tissues in a noninvasive and harm-free fashion.

DOI: [10.1103/PhysRevA.107.032611](https://doi.org/10.1103/PhysRevA.107.032611)

### I. INTRODUCTION

Quantum imaging is a method that creates images from objects thanks to entangled beams, which can even produce images by a light that has never physically interacted with the object [1–3]; this is one of the unique and essential points of this imaging method. Some important quantum imaging techniques are ghost imaging, lithography, and quantum sensing. These methods use quantum correlations between entangled photon pairs. Correlation is one of the basic features of quantum mechanics, which improves image resolution compared to classical imaging [4]. Quantum and classical spatial correlations can be considered a gateway for developing quantum imaging techniques. For this reason, measuring and studying the correlation between photon pairs in quantum systems is one of the most important topics in quantum imaging, quantum information, and computation [5,6]. To create entanglement between two photons, we need a nonlinear factor by which the two produced photons do not follow Maxwell's linear equations and provide a nonlinear optical field. The two entangled photons are completely correlated so that by examining the information of one beam, the information of the other beam can be obtained. It should be noted that this complete correlation is not created by the classical source. One of the most important processes that produces two entangled beams from another input beam is the spontaneous parametric down-conversion (SPDC) process in which a laser light passes through a nonlinear crystal, e.g., beta barium borate (BBO), and is then separated into two entangled beams. Basically, quantum imaging protocols use two-arm configurations, where in one arm a single-pixel detector is

placed in front of the object, and in the other arm a multipixel scan detector that does not see the object is used. According to this configuration, the arm in which the object is located is called the signal arm and the other arm is called the reference arm. The object is illuminated by the signal beam, and the idler beam is sent in the reference arm as a quantum copy of the signal beam, but received by another detector. Finally, the image intensity of the quantum imaging method is obtained by using the convolution between the object distribution function and a second-order point-to-point correlation function between the two detectors [6–8].

### II. PROPOSAL FOR HIGH-CONTRAST INTERACTION-FREE QUANTUM IMAGING METHOD

Here, we would like to propose an imaging technique, using the correlation-based quantum imaging (CBQI) and interaction-free ghost imaging (IFGI) methods, to see whether a new quantum optical method is possible for imaging with fewer photons than conventional imaging techniques, but with better visibility and resolution even if the detected photons did not previously interact with the object in a noisy environment [9]. To realize this purpose, we use the interaction-free ghost imaging method, which was recently introduced and performed in experiments [10,11].

#### A. Correlation-based quantum imaging (CBQI)

In imaging systems, when a low-reflection target is placed in environments with high levels of loss and noise, the noise photons will overwhelm the original signal photons at the receiver due to low initial power. Therefore, the probability of error increases as noise photons are detected at the receiver, implying that an object is present even if it is not. In this case, target detection can be a big problem. Entanglement can be

\*shabir.barzanjeh@ucalgary.ca

†vahid.salari@ucalgary.ca

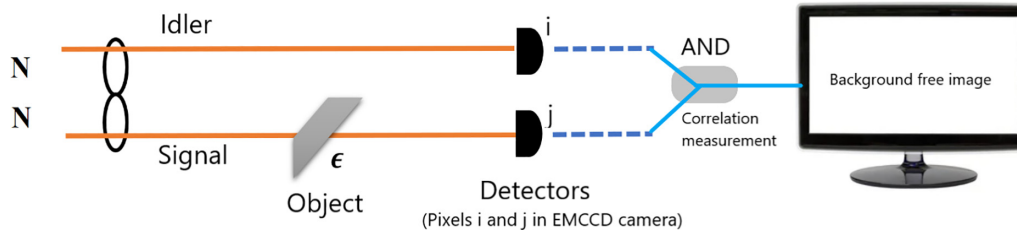


FIG. 1. A simple demonstration of the correlation-based quantum imaging (CBQI) protocol when one of the entangled beams (i.e., signal) is illuminated to an object with transmissivity  $\epsilon$  and the other one (i.e., idler) remains intact. This is similar to the quantum illumination setup that only determines whether or not there is a target, and this correlation-based imaging method is different from the quantum radar concept in terms of continuous variables (e.g., two-mode squeezed states) [12–15].

used to better distinguish between noise photons and signal photons and decrease the probability of error. For instance, the quantum illumination protocol is used to detect the presence or absence of a low-reflection object located in a noisy environment [12]. In this method, the signal beam directly illuminates the object and the idler beam is retained for use in a joint measurement on the return signal. Then, if part of the signal is reflected, it indicates that an object is present, otherwise there was no object. It should be noted that most of the signal is often lost, and if there is an object, only a small part of it returns. When the signal beam illuminates the object, the object is immersed in thermal radiations and noise, so we must be able to distinguish all reflected light from the background of the noise. Therefore, if two entangled beams of the signal and idler are used in this method and then a quantum measurement is performed on the return beam from the object and the idler beam, the quantum process will be more sensitive. In our imaging technique, we assume that the reflectivity of the object can be replaced with the transmissivity of that versus the signal beam (see Fig. 1).

Recently, Padgett *et al.* have performed imaging via correlation-based quantum imaging and obtained significant quantum advantage [5]. In their experiment, spatial quantum correlations were used in entangled photon pairs generated by the SPDC process. Both beams are received by different regions of an electron-multiplying CCD (EMCCD) array detector. EMCCD has a benefit to obtain the correlation between each pair of rays that is received in the detector arrays. In fact, AND operations [5] are used to improve the image quality and visibility. This pixel-by-pixel operation is performed between two regions of the array detectors that have received SPDC rays, to choose the preferable pair of correlated photons, and reject the sensor noise and uncorrelated background light. The result will be that the correlation-based quantum imaging AND image resulting from the sum of the AND operations will have a better visibility than the classical image that includes both sensor noise events and background illumination events; also, the final correlation-based quantum imaging AND images will have no background. It is important to note that although, in the presence of high noise and loss, both images obtained from conventional and correlation-based quantum imaging AND methods are affected, the correlation-based quantum imaging protocol performs better than a conventional one. Additionally, by increasing the levels of thermal illumination, the correlation-based quantum imaging AND image has better visibility compared with the

conventional image. Moreover, by adding losses to the imaging operation, the visibility of the image obtained by the AND operation will drop much slower than the visibility of the conventional image.

In the following, we will show that how we use the benefit of the CBQI method in our imaging protocol.

### B. Interaction-free ghost imaging (IFGI)

Researchers have always sought to improve the resolution of the images and have proposed various experiments and configurations to achieve it. One idea is to merge the two methods of interaction-free imaging and ghost imaging [2,3,10,16], i.e., called interaction-free ghost imaging, which has the advantages of both methods.

Generally, the interaction-free technique is a detection method involving a single photon passing through the interferometer to reveal the presence of an object placed in one of the interferometer's arms. If no object exists in one of the interferometer arms, then the photon interferes constructively with itself and is received only by one exit port. On the other hand, if the object is placed in an interferometer arm, the photon interference is disturbed and it is possible to receive photons from both exit ports. Placing an object in an interferometer arm changes the path difference between two beams and the interference pattern. Therefore, the second exit port only receives photons if an object is in one of the interferometer arms. The strength of this method is that this photon never interacts with the object, but can detect its presence. On the other hand, conventional ghost imaging uses entangled photon pairs from the SPDC process to capture from an object. In this configuration, one entangled photon illuminates the object and is detected by a bucket detector, and another one without any interaction is sent to a camera. Finally, by measuring the coincidence photons at these two detectors, an image is produced on the camera.

For the IFGI configuration, as shown in Fig. 2, an entangled photon pair from the SPDC process is separated into signal and idler beams by a 50/50 beam splitter. A Mach-Zehnder interferometer is placed along the path of the signal beam, and a bucket detector is used at each of the interferometer's two output ports. As explained, if there is no object in the interferometer arms, then the photon interference is constructive and is recorded only in detector  $D_3$ , called a constructive detector. Still, if an object exists in one of the interferometer arms, the photon interference is destructive and both bucket detectors

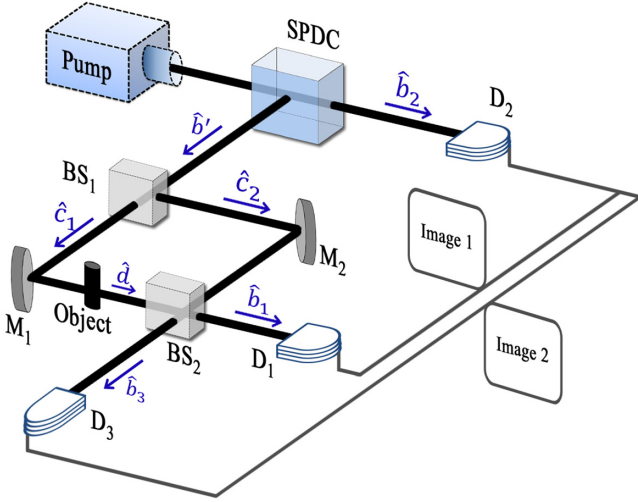


FIG. 2. Interaction-free ghost imaging (IFGI) protocol. Entangled photons are produced during the SPDC process and separated into signal  $\hat{b}$  and idler  $\hat{b}'$  fields. The operators  $\hat{c}_1$  and  $\hat{c}_2$  passed the two interferometer arms by acting the signal field on BS1. Then the operator  $\hat{c}_1$  acts on the object with transmission  $\epsilon$ , and two operators  $\hat{c}_2$  and  $\hat{d}$  interact with each other on BS2. Finally, two fields  $\hat{b}_1$  and  $\hat{b}'$  are received by detector  $D_1$  and  $D_3$ , respectively. Image 1 is obtained from measuring coincidence photons between destructive detector  $D_1$  and detector  $D_2$ , and similarly image 2 is obtained from measuring coincidence photons between constructive detector  $D_3$  and detector  $D_2$ .

may detect photons. Further, the idler beam is received by  $D_2$ , triggered once by constructive bucket detector  $D_3$  and another time with destructive bucket detector  $D_1$  to measure coincidence photons between the signal and idler beams and create two images. Finally, two images are obtained from two interferometer's output ports by subtracting them from each other; even though fewer photons illuminate the object, we can get an image with the same or even better quality than conventional ghost imaging. This feature can be essential in imaging objects susceptible to light, such as some biological tissues.

To investigate the formed image using any quantum imaging techniques, it is necessary to calculate the most significant parameter, i.e., the signal-to-noise ratio (SNR). The SNR can be defined as the ratio of the mean contrast to its standard deviation,

$$\text{SNR} = \frac{|\langle S_{\text{in}} - S_{\text{out}} \rangle|}{\sqrt{\langle \delta^2(S_{\text{in}} - S_{\text{out}}) \rangle}}, \quad (1)$$

where  $\delta S = S - \langle S \rangle$  is the standard deviation and  $\langle \rangle$  represents the theoretical expectation value. Here,  $S_{\text{in}}(S_{\text{out}})$  is the photon-number correlation function between the total photon numbers of the signal and idler at their detectors for a set of  $M$  times when the object is placed in the interferometer (there is no object) [17],

$$S = G^{(2)}(x) \equiv E[N_i N_j(x)] = E[\hat{b}_i^+ \hat{b}_i \hat{b}_j^+ \hat{b}_j], \quad (2)$$

where  $G^{(2)}(x)$  is the second-order correlation function between the intensities,  $N_i = \hat{b}_i^+ \hat{b}_i$  is the total number of the signal photon which is detected by the bucket detector  $D_i$ ,

$N_j(x) = \hat{b}_j^+ \hat{b}_j$  is the total number of idler photons, which is detected at point  $x$  in the camera  $D_j$ , and  $E[x] = \frac{1}{M} \sum_{m=1}^M x^m$  is the average over the set of  $M$  frames. As shown in Fig. 2, in the presence of an object, two images of the object are reconstructed from two outputs, once by measuring the correlation function  $G^{(2)}(x)$  between  $N_1$  and  $N_2(x)$  which produces image 1, and another time between  $N_3$ , the total number of photons collected at the bucket detector  $D_3$ , and  $N_2(x)$  which produces image 2.

Now we start from the SPDC Hamiltonian and the relation between the input and output of the signal and idler fields produced from the SPDC process to obtain the signal and idler operators at their detector's plane. The SPDC Hamiltonian is written as below [18–21],

$$\hat{H}_{\text{SPDC}} = \sum_{k,\omega} i\hbar\zeta(k_P, \omega_P)(\hat{a}_1^+(k_s, \omega_s)\hat{a}_2^+(k_i, \omega_i) + \text{H.c.}), \quad (3)$$

where the operator  $\hat{a}_i^+$  is the creation operator of the signal ( $i = 1$ ) and idler ( $i = 2$ ) at the input face of the crystal and  $\zeta(k, \omega)$  corresponds to the pump beam power. Also,  $k_{p,s,i}$  and  $\omega_{p,s,i}$  are the transverse wave vector and frequency of the pump, signal, and idler, respectively. By substituting the detuning frequency of the signal and idler photons  $\omega$  from the central pump frequency  $\frac{\omega_P}{2}$  and the symmetric and correlated transverse wave vector  $k$ , we can rewrite the Hamiltonian,

$$\hat{H}_{\text{SPDC}} = \sum_{k,\omega} i\hbar[\zeta\hat{a}_1^+(k, \omega)\hat{a}_2^+(-k, -\omega) + \text{H.c.}]. \quad (4)$$

Now the operator of signal  $\hat{b}(k, \omega)$  and idler  $\hat{b}_2(k, \omega)$  at the output face of the crystal can be defined [22,23],

$$\hat{b}_2(k, \omega) = U(\zeta)\hat{a}_1(k, \omega) + V(\zeta)\hat{a}_2^+(-k, -\omega), \quad (5)$$

$$\hat{b}(k, \omega) = U(\zeta)\hat{a}_2(k, \omega) + V(\zeta)\hat{a}_1^+(-k, -\omega), \quad (6)$$

where  $U(\zeta) = \cosh(\zeta)$  and  $V(\zeta) = \sinh(\zeta)$ , and the mean photon number is  $\bar{N} = V(\zeta)^2$ . Now the operators  $\hat{c}_1(k, \omega)$  and  $\hat{c}_2(k, \omega)$  after the first beam splitter are given by

$$\hat{c}_1(k, \omega) = \sqrt{T}\hat{b}(k, \omega) + i\sqrt{R}\hat{v}, \quad (7)$$

$$\hat{c}_2(k, \omega) = \sqrt{T}\hat{v} + i\sqrt{R}\hat{b}(k, \omega). \quad (8)$$

Here,  $\hat{v}$  is the annihilation vacuum field, and  $T$  and  $R$  are the transmission and reflection coefficients where  $R + T = 1$ . As the object is placed in one arm of the interferometer, the operator  $\hat{c}_1(k, \omega)$  acts on the object with transmission  $\epsilon$ , so we have

$$\hat{d}(k, \omega) = \sqrt{\epsilon}\hat{c}_1(k, \omega) + i\sqrt{1-\epsilon}\hat{v}', \quad (9)$$

where  $\hat{v}'$  is an annihilation vacuum field. Finally, two interaction beams  $\hat{c}_2(k, \omega)$  and  $\hat{d}(k, \omega)$  act on BS2 and two signal detection fields on the  $D_1$  and  $D_3$  detector planes are given by

$$\hat{b}_1(k, \omega) = \sqrt{R}\hat{d}(k, \omega) + i\sqrt{T}\hat{c}_2(k, \omega), \quad (10)$$

$$\hat{b}_3(k, \omega) = \sqrt{R}\hat{c}_2(k, \omega) + i\sqrt{T}\hat{d}(k, \omega). \quad (11)$$

At this point, the evaluation of the photon-number correlation and its fluctuation requires expressions for the first-

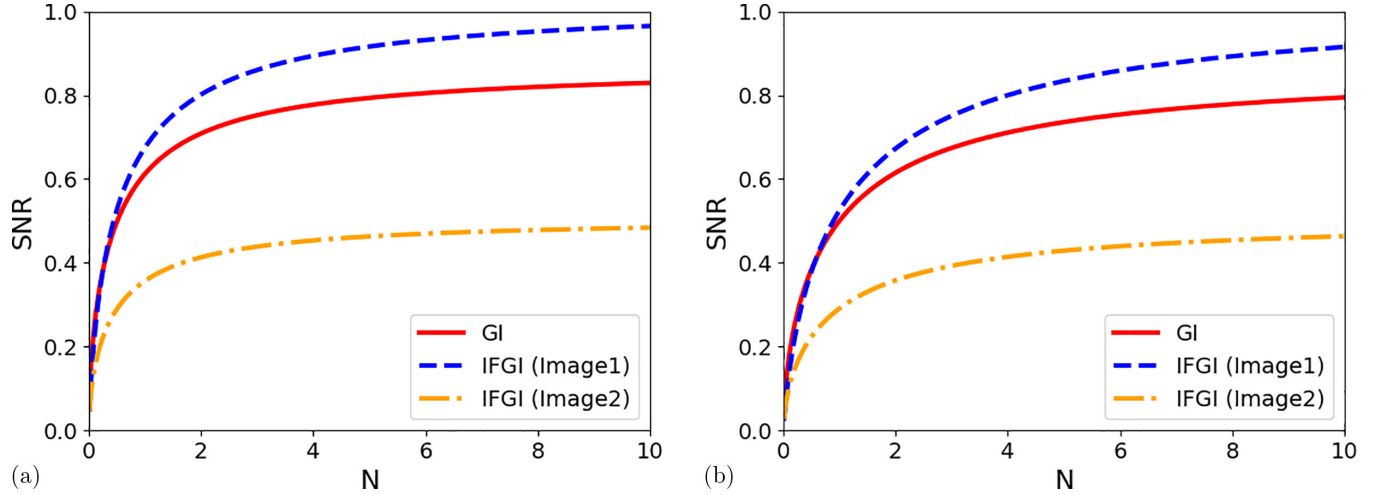


FIG. 3. The SNRs for the obtained images from ghost imaging (GI) and interaction-free ghost imaging (IFGI) techniques, plotted as a function of mean photon number  $\bar{N}$ . The red solid line corresponds to the GI image, the blue dashed line corresponds to the destructive output of IFGI setup  $D_1$ , and the yellow dash-dotted line corresponds to the constructive output of IFGI setup  $D_3$ . The SNRs are determined with the BS transmission and reflectivity coefficients  $R = T = 0.5$  and  $\epsilon = 0.1$ , (a)  $\eta = 1.0$  and (b)  $\eta = 0.5$ .

fourth-order moments of the intensity. Brida *et al.* obtained the correlation between the readings of the bucket detector and those of an arbitrary pixel in the reference arm for GI protocol [21]. It is enough for the IFGI setup, which includes an interferometer, to substitute the single-mode photon-number statistics with the above relations. According to the IFGI setup, the single-mode photon-number statistics for each detector is given by

$$\langle n_1 \rangle = \eta_1 \bar{N} (\sqrt{\epsilon RT} - \sqrt{RT})^2, \quad (12)$$

$$\langle n_2 \rangle = \eta_2 \bar{N}, \quad (13)$$

$$\langle n_3 \rangle = \eta_1 \bar{N} (R + T \sqrt{\epsilon})^2, \quad (14)$$

where  $\eta_{1,2}$  is the efficiency of the signal and reference arm, respectively. Therefore, the higher-order moments are written as below,

$$\langle n_1^2 \rangle = \eta_1 \bar{N} (\sqrt{\epsilon RT} - \sqrt{RT})^2 + 2\eta_1^2 \bar{N}^2 (\sqrt{\epsilon RT} - \sqrt{RT})^4, \quad (15)$$

$$\langle n_2^2 \rangle = \eta_2 \bar{N} + 2\eta_2^2 \bar{N}^2, \quad (16)$$

$$\langle n_3^2 \rangle = \eta_1 \bar{N} (R + T \sqrt{\epsilon})^2 + 2\eta_1^2 \bar{N}^2 (R + T \sqrt{\epsilon})^4, \quad (17)$$

$$\langle n_1 n_2 \rangle = \eta_1 \eta_2 (2\bar{N}^2 + \bar{N}) (\sqrt{\epsilon RT} - \sqrt{RT})^2, \quad (18)$$

$$\langle n_3 n_2 \rangle = \eta_1 \eta_2 (2\bar{N}^2 + \bar{N}) (R + T \sqrt{\epsilon})^2, \quad (19)$$

$$\langle n_1^2 n_2 \rangle = \eta_1 \eta_2 (2\bar{N}^2 + \bar{N}) (\sqrt{\epsilon RT} - \sqrt{RT})^2 + \eta_1^2 \eta_2 (6\bar{N}^3 + 4\bar{N}^2) (\sqrt{\epsilon RT} - \sqrt{RT})^4, \quad (20)$$

$$\langle n_3^2 n_2 \rangle = \eta_1 \eta_2 (2\bar{N}^2 + \bar{N}) (R + T \sqrt{\epsilon})^2 + \eta_1^2 \eta_2 (6\bar{N}^3 + 4\bar{N}^2) (R + T \sqrt{\epsilon})^4, \quad (21)$$

$$\begin{aligned} \langle n_1^2 n_2^2 \rangle &= \eta_1 \eta_2 (2\bar{N}^2 + \bar{N}) (\sqrt{\epsilon RT} - \sqrt{RT})^2 \\ &\quad + \eta_1^2 \eta_2 (6\bar{N}^3 + 4\bar{N}^2) (\sqrt{\epsilon RT} - \sqrt{RT})^4 \\ &\quad + \eta_1 \eta_2^2 (6\bar{N}^3 + 4\bar{N}^2) (\sqrt{\epsilon RT} - \sqrt{RT})^2 \\ &\quad + \eta_1^2 \eta_2^2 (24\bar{N}^4 + 24\bar{N}^3 + 4\bar{N}^2) (\sqrt{\epsilon RT} - \sqrt{RT})^4, \end{aligned} \quad (22)$$

$$\begin{aligned} \langle n_3^2 n_2^2 \rangle &= \eta_1 \eta_2 (2\bar{N}^2 + \bar{N}) (R + T \sqrt{\epsilon})^2 \\ &\quad + \eta_1^2 \eta_2 (6\bar{N}^3 + 4\bar{N}^2) (R + T \sqrt{\epsilon})^4 \\ &\quad + \eta_1 \eta_2^2 (6\bar{N}^3 + 4\bar{N}^2) (R + T \sqrt{\epsilon})^2 \\ &\quad + \eta_1^2 \eta_2^2 (24\bar{N}^4 + 24\bar{N}^3 + 4\bar{N}^2) (R + T \sqrt{\epsilon})^4. \end{aligned} \quad (23)$$

Now we consider an ideal case of the quantum efficiency in both arms,  $\eta_1 = \eta_2 = \eta$ , and the transmission and reflection coefficients  $R = T = 0.5$ . Figure 3 represents the SNRs for the GI and IFGI images as a function of the mean photon number. As can be seen, image 1, produced by measuring the photon-number correlation function between detectors  $D_2$  and  $D_1$ , has a significantly higher SNR than the GI image even with less mean photon number, and this advantage is preserved by increasing the mean photon number. Therefore, the use of an interferometer in the configuration of the quantum imaging system can prevent the destruction of the sample due to collision with a large number of photons. Also, its image from destructive output has a higher resolution. As a significant result, we propose to use an interferometer in a correlation-based quantum imaging setup to achieve these advantages.

### C. Interaction-free quantum imaging (IFQI) method

Now we are at the point of introducing our proposed method utilizing CBQI and IFGI methods in a merged setup. The technique of CBQI here is mainly based on the quantum correlations between entangled beams and removing

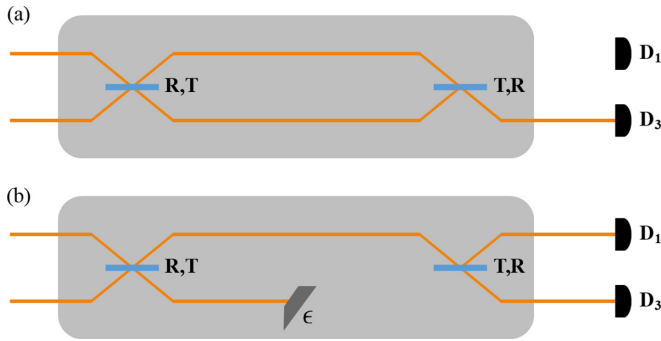


FIG. 4. The diagram indicates passing photons in the absence and presence of the object in the interferometer. For simplicity, we assume  $R_1 = T_2 = R$  and  $T_1 = R_2 = T$ . (a) For the absence of the object, the photon has entered the interferometer and is received by constructive detector ( $D_3$ ). (b) When the object is located in one of interferometer arms, the input photon may be detected in both the constructive detector ( $D_3$ ) and destructive detector ( $D_1$ ).

thermal noise due to no correlations with entangled beams, to have a higher SNR and visibility for the imaging of the object [5]. We call our suggested technique interaction-free correlation-based quantum imaging (CBQI) and elaborate it in the following. As you can see in Fig. 5, we use pairs of entangled photons that were produced by the SPDC process. Two beams, the signal and idler, are transmitted to the detectors in separated paths. In the path of the signal beam, we use an optical interferometer [i.e., an asymmetric Mach-Zehnder interferometer (MZI)], where an object is placed in one of the arms of the MZI. Then we place a bucket detector in the path of each of the interferometer outputs to receive the output beams from each port.

Depending on the presence or absence of the object, the photon passing through the interferometer is received by  $D_1$  or  $D_3$ . As you can see in Fig. 4(a), if the object is not present, the photons in the interferometer will interfere with each other

and all of them will be received by  $D_3$ ; in other words, no photon will be received by  $D_1$ . Under these conditions, the probability of detecting a single photon will be  $P(D_3) = 1$  and  $P(D_1) = 0$ . But if the target is placed in one of the interferometer arms, as shown in Fig. 4(b), then the interference will be disturbed and the output photons from the interferometer may be received by both detectors. Two detectors,  $D_3$  and  $D_1$ , show us the constructive and destructive interferences and are called the constructive and destructive exit ports, respectively. If the first and second beam splitters in the interferometer have reflectivity  $R_1$  and  $R_2$ , and transmissivity  $T_1$  and  $T_2$ , respectively, then the detection probability by  $D_3$  will be  $P(D_3) = R_1 T_2$ . This detection is caused by the first BS reflection and second BS transmission. We should note that  $D_3$  does not give us information about the presence or absence of the object because this detector can detect, in both cases, the presence and absence of the object. In fact, in this experiment, the detection of  $D_1$  is important to us because only then we will find out that there was an object in the interferometer arm. This detection occurs when the first and second BSs reflect a photon, so the probability of that is  $P(D_1) = R_1 R_2$ . The important point is that no photon is absorbed by the object because we have sent only one photon into the interferometer and it has been received by  $D_1$ . This is why we call this method interaction free, because the presence of an object is determined without the direct interaction of the detected photon with the object (see Fig. 6).

The advantage of using an interferometer is that fewer photons interact with the object and images with the same or even better resolution will be produced, compared to correlation-based quantum imaging. For example, in correlation-based quantum imaging, if an average of  $\bar{N}$  photons enter an interferometer to detect the object, when there is no object, all the  $\bar{N}$  photons will be received by a detector and, in the presence of the object, all the  $\bar{N}$  photons will be absorbed or scattered by the object. Therefore, the difference between the number of photons received in the presence and absence of the object in the detector will be  $\Delta N_C = -\bar{N}$ .

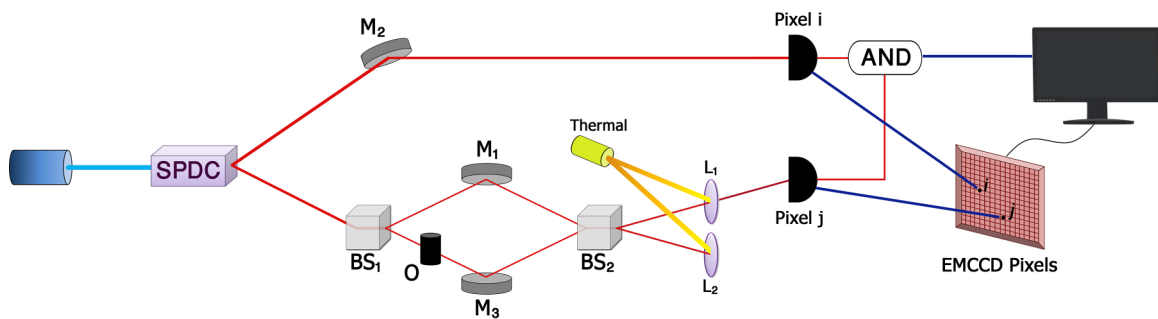


FIG. 5. Experimental setup of IFQI. In this scheme,  $M_1$ ,  $M_2$ , and  $M_3$  are mirrors and  $BS_1$  and  $BS_2$  are beam splitters in the interferometer. A BBO crystal is pumped by a laser beam to produce entangled photon pairs via the SPDC process. One photon is sent into an interferometer with the object to be interrogated; the second photon is sent to a detector where the image of the object is formed. The thermal background is sent to the two lenses  $L_1$  and  $L_2$  to overlays the signal beam, and then received by two detectors  $D_1$  and  $D_3$ . On the other hand, in the other arm, the idler beam is received by the  $D_2$  detector. Then, in order to increase the resolution and remove the background, AND operations are performed on the obtained data from both detectors. In fact, each single pixel is a single-photon detector and in each time step only two photons click on two random pixels (e.g., pixels  $i$  and  $j$ ) and the EMCCD camera can measure the correlations between each of the two incident photons. If the correlations approach zero (e.g., between a thermal noise photon and a signal photon), then the AND algorithm ignores them. If there is significant correlation, the algorithm keeps them.

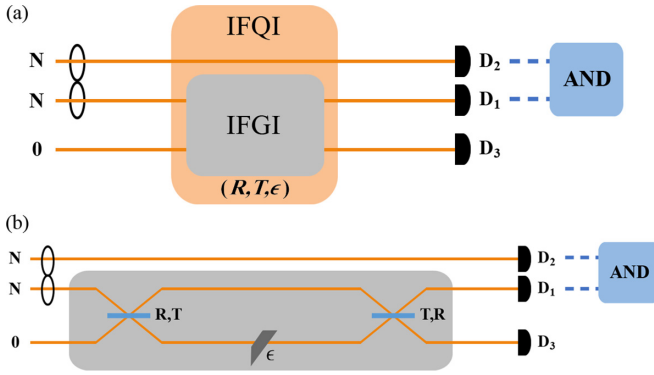


FIG. 6. (a) The interaction-free quantum imaging (IFQI) setup takes the role of the idler beam at  $D_2$  into account. The correlation between the signal and the idler beams at  $D_1, D_2$  is analyzed via the AND algorithm, and (b) the IFQI protocol with a transparent IFGI box. The advantage of using IFGI in the correlation-based quantum imaging method is forming images with a lower number of photons but with higher visibility, even with the feasibility of the formation of the images with photons that never interacted with the target.

### III. ASSESSMENT OF THE OUTPUTS: SIGNAL-TO-NOISE RATIO (SNR), VISIBILITY, POWER, AND ADVANTAGE

The clarity of the image details is a very important feature of each imaging technique. For imaging methods, from the smallest details to the largest parts of the image, all depend on the parameters of the imaging technique that we use. We intend to study the general parameters of quantum imaging and their relation to other image characteristics. The quantity of the signal-to-noise ratio is one of these parameters that we are interested in examining. In fact, this parameter is a criterion that compares the desired signal level to the background noise and is defined as the ratio of signal power to noise power. The unit of this quantity is decibels and its mathematical definition can be expressed as follows:

$$\text{SNR} = \frac{|\Delta I|}{\sigma(\Delta I)}, \quad (24)$$

where  $\Delta I = I_{\text{in}} - I_{\text{out}}$  is the difference of the average intensity values, inside and outside the object profile, respectively, and  $\sigma := \sigma(I_{\text{in}} - I_{\text{out}})$  is the standard deviation of this difference. From the above definition, it is understood that if the value of this parameter is high, the images will have better resolution.

Another important parameter in quantum imaging is visibility. This quantity indicates that the image of the object is how recognizable it is from the background. If we consider  $I_{\text{max}}$  as the number of reflected photons from an object, i.e., the bright area intensity of the image, and  $I_{\text{min}}$  as the number of photons left from the beam that are not reflected and produce the background, i.e., the dark area intensity of the image, then the image visibility can be defined as follows:

$$V = \frac{I_{\text{max}} - I_{\text{min}}}{I_{\text{max}} + I_{\text{min}}}. \quad (25)$$

Obviously, if the value of this parameter is high, then the image visibility will be better. Therefore, each imaging method that has a better signal-to-noise ratio and visibility

will be a more desirable method for performing the imaging process.

In the interaction-free protocol as shown in Fig. 4, for simplicity, we assume  $R_1 = T_2 = R$  and  $T_1 = R_2 = T$ , so if an average of  $\bar{N}$  photons enter the interferometer, in the absence of the object,  $\bar{N}$  photons will be received by the constructive interference exit port and no photons will be received by another one. On the other hand, in the presence of the object,  $\bar{N}R^2$  photons are detected by the constructive exit port and  $\bar{N}RT = \bar{N}R(1 - R)$  photons are received by the destructive exit port. Therefore, for the IFQI method, a change in photon number at the constructive and destructive exit port is  $\bar{N}R^2 - \bar{N}$  and  $\bar{N}RT$ , respectively. Now, if we subtract these changes, then the change in number of the received photon in the IFQI method can be calculated as follows:

$$\Delta N_{\text{IFQI}} = \bar{N}(R^2 - RT - 1). \quad (26)$$

For the values of  $R = T = 0.5$ , the change in number of photons in the IFQI and CBQI is equal,  $\Delta N_{\text{IFQI}} = \Delta N_{\text{C}}$ , i.e., the number of received photons by the detectors will be the same in both methods, but in the IFQI, we see that half the number of photons interact with the object compared to CBQI. Therefore, by using an interferometer, the same number of received photons can be obtained with a smaller number of interacting photons.

In an experimental setup, background light and environmental noise affect the image properties such as SNR and visibility. Therefore, in order to simulate the real-world conditions, we use a thermal light as the incoming background light to overlay the signal beams at both  $D_1$  and  $D_3$ . In fact, because thermal light has a similar distribution to environmental noise, we use thermal light as a background light. Now in order to eliminate image backgrounds and have better performance in noisy environments, we use an advanced detection protocol by the AND operation.

This pixel-by-pixel operation is performed between the two regions of  $D_2$  and  $D_1$ . In this operation, pairs of correlated photons are preferably selected and uncorrelated background light and noise are not considered. Then we add the data in opposite positions of the correlation peak within the same frame to create an AND image. Finally, we perform the AND operation on a number of frames and collect all the obtained images together to form the final IFQI image.

*Conventional method.* In the conventional method, the acquired image is produced by the simple sum of the raw data. Since this image is obtained without using AND operations (or quantum correlations), we may call it somehow as a conventional image.

In the next sections, we will see that an AND image, i.e., constructed by summing the results of AND operations, has a better resolution and visibility than the conventional image because, unlike the conventional image, it contains correlated data and does not include noise and background light. In fact, this advantage is due to the preferential selection of correlated photon pairs and the elimination of uncorrelated photons due to noise or background light. It is important to note that in the presence of noise and loss, this advantage of the IFQI protocol is maintained. Our expectation of the IFQI method is increasing the resolution and visibility of images with fewer

interactive photons, performing better in noisy environments, and rejecting backgrounds.

In order to analyze the benefits of using the AND operation in the quality of the images, we need to determine the SNR of the IFQI image through the AND operation and conventionally acquired image. So we present the description of both the IFQI image and the conventionally acquired image theoretically. We define two image variables from two exit ports, as shown in Fig. 5. For simplicity, we assume a Mach-Zehnder interferometer with the input BS having reflectivity  $R$  and transmissivity  $T$ , and the exit BS having reflectivity  $T$  and transmissivity  $R$ . We note  $\eta$  as the apparatus arm efficiency, i.e., including losses occurring during the correlation-based quantum imaging. So that, if the efficiency of the reference arm from the crystal to the camera is  $\eta$ , and if the object reflectivity is  $\epsilon$ , then the signal arm efficiency from the crystal to the camera will be  $\epsilon\eta$ . Also, we define  $d$  as the dark count and  $\mathcal{T}$  the thermal light in the signal arm to measure the ability of our IFQI scheme under different thermal light and noise levels.

In general, if an average of  $\bar{N}$  photons enters each signal and the reference arm from the SPDC process, then in the absence of an object,  $\bar{N}$  photons will be detected in one of the exit ports. Therefore, in the presence of both noise and losses, the photon number in the  $D_1$  and  $D_2$  exit ports of a conventionally acquired image is  $N_{D_2(\epsilon=1)}^C = \bar{N} + \mathcal{T} + d$  and  $N_{D_1(\epsilon=1)}^C = \mathcal{T} + d$ . Also, if the object is placed in the transmission arm of the interferometer, then the photon number in each exit port will be  $N_{D_2(\epsilon \neq 1)}^C = \bar{N}R^2 + \epsilon\bar{N}T^2 + \mathcal{T} + d$  and  $N_{D_1(\epsilon \neq 1)}^C = \bar{N}RT + \epsilon\bar{N}RT + \mathcal{T} + d$ . Therefore, a change in photon number will be  $\Delta N_{D_2}^C = \bar{N}R^2 + \epsilon\bar{N}T^2 - \bar{N}$  and  $\Delta N_{D_1}^C = \bar{N}RT + \epsilon\bar{N}RT$ . Subtracting  $\Delta N_{D_1}^C$  from  $\Delta N_{D_2}^C$  gives  $|\Delta N_{D_2}^C - \Delta N_{D_1}^C| = \bar{N}R^2 + \epsilon\bar{N}T^2 - \bar{N} - (\bar{N}RT + \epsilon\bar{N}RT)$ . As the SPDC has Poissonian statistics in the coincidence count, the standard deviation is then  $\sigma(\Delta N_{D_2}^C - \Delta N_{D_1}^C) = \bar{N}R^2 + \epsilon\bar{N}T^2 + \bar{N} + (\bar{N}RT + \epsilon\bar{N}RT)$ .

One can as well express the photon number of the IFQI image [5], i.e.,  $N^Q = \epsilon\eta N + [N(1 - \epsilon\eta) + d][\epsilon N(1 - \eta) + d + \mathcal{T}]$ .

The photon number in each exit port in the absence of the object is as follows:  $N_{D_2(\epsilon=1)}^Q = \eta\bar{N} + [\bar{N}(1 - \eta) + d][\bar{N}(1 - \eta) + \mathcal{T} + d]$  and  $N_{D_1(\epsilon=1)}^Q = [\bar{N}(1 - \eta) + d](\mathcal{T} + d)$ . And for the case in which an object is placed in the transmission arm of the interferometer, the photon number is  $N_{D_2(\epsilon \neq 1)}^Q = (R^2 + \epsilon T^2)\eta\bar{N} + \{\bar{N}[1 - (R^2 + \epsilon T^2)\eta] + d\}[\bar{N}(R^2 + \epsilon T^2)(1 - \eta) + \mathcal{T} + d]$  and  $N_{D_1(\epsilon \neq 1)}^Q = (RT + \epsilon RT)\eta\bar{N} + \{\bar{N}[1 - (RT + \epsilon RT)\eta] + d\}[\bar{N}(RT + \epsilon RT)(1 - \eta) + \mathcal{T} + d]$ . Now from these equations, the SNR of the IFQI image and the conventionally acquired image can be determined by  $\text{SNR} = \frac{|\Delta N|}{\sigma(\Delta N)}$ ,

$$\begin{aligned} \text{SNR}_C &= \frac{|\Delta N_{D_2}^C - \Delta N_{D_1}^C|}{\sqrt{\sigma^2(\Delta N_{D_2}^C - \Delta N_{D_1}^C)}} \\ &= \frac{|(N_{D_2(\epsilon \neq 1)}^C - N_{D_2(\epsilon=1)}^C) - (N_{D_1(\epsilon \neq 1)}^C - N_{D_1(\epsilon=1)}^C)|}{N_{D_2(\epsilon \neq 1)}^C + N_{D_2(\epsilon=1)}^C + N_{D_1(\epsilon \neq 1)}^C + N_{D_1(\epsilon=1)}^C}, \end{aligned} \quad (27)$$

$$\begin{aligned} \text{SNR}_Q &= \frac{|\Delta N_{D_2}^Q - \Delta N_{D_1}^Q|}{\sqrt{\sigma^2(\Delta N_{D_2}^Q - \Delta N_{D_1}^Q)}} \\ &= \frac{|(N_{D_2(\epsilon \neq 1)}^Q - N_{D_2(\epsilon=1)}^Q) - (N_{D_1(\epsilon \neq 1)}^Q - N_{D_1(\epsilon=1)}^Q)|}{N_{D_2(\epsilon \neq 1)}^Q + N_{D_2(\epsilon=1)}^Q + N_{D_1(\epsilon \neq 1)}^Q + N_{D_1(\epsilon=1)}^Q}. \end{aligned} \quad (28)$$

The SNRs for both the conventionally acquired image and the IFQI image are demonstrated theoretically in Fig. 7, where within the same interrogation time, we assume for Fig. 7(a), on average,  $\bar{N} = 0.5$ , and for Fig. 7(b),  $\bar{N} = 10$  photons enter the interferometer, and the thermal light and the dark count are  $\mathcal{T} = 10$  and  $d = 10$ . Our main focus in the IFQI technique is on the objects that have low reflectivity and also noisy environments, so we assume a very small value for  $\epsilon$  and  $\eta$ . Figure 7 shows that by the fewer photons interacting with the object, the IFQI image has a better SNR than the conventional one, even when the thermal light and the dark count are very high. This advantage is due to the fact that the AND operation will preferentially keep the photon pairs and will reject most of the uncorrelated ones that arise from either environmental noise or unwanted background illumination. From these results, we can verify that as the number of entire photons,  $\bar{N}$ , increases, this improvement in quantum image resolution increases compared to the conventional one.

Here, we observe that the SNR improvement of the IFQI image holds a maximum value, when  $R = 0.24$ . Now we can investigate the SNR treatment as a function of other parameters at this optimal  $R$ . To demonstrate the SNR improvement of IFQI under the thermal light and the noise, we define the power  $P$  as the ratio between the IFQI SNR through the AND operation (i.e., the image obtained by keeping only the correlated photons through performing the AND operation) and the SNR of the conventionally acquired image (i.e., the image acquired simply by summing the signal beam photons),

$$P = \frac{\text{SNR}_Q}{\text{SNR}_C} \quad (29)$$

It is also possible to discuss the power  $P$  as a function of  $\mathcal{T}$ ,  $\eta$ , and  $\epsilon$ . As shown in Fig. 8, the power decreases with increasing  $\eta$ . Therefore, we can understand, when environmental noise is very high, i.e.,  $\eta$  is small, that the IFQI SNR through the AND operation will be approximately three times better than the conventional SNR. It is important to note that the advantage of the IFQI SNR through the AND operation compared to the classic is maintained with the addition of thermal light.

From the image presented in Fig. 9, it is seen that the power increases with the level of the object reflectivity,  $\epsilon$ . Obviously, imaging the object with higher reflectivity produces images with better SNR, but using the AND operation can enhance the SNR more. We should note that in noisy environment, i.e.,  $\eta < 0.4$ , the IFQI image has a better SNR than the conventional one for low-reflectivity objects.

In order to demonstrate the advantage of using the AND operation in our IFQI scheme to reject the background thermal light and noise, we have to measure the advantage  $A$ , which is defined in Ref. [5]. This quantity is the ratio between the

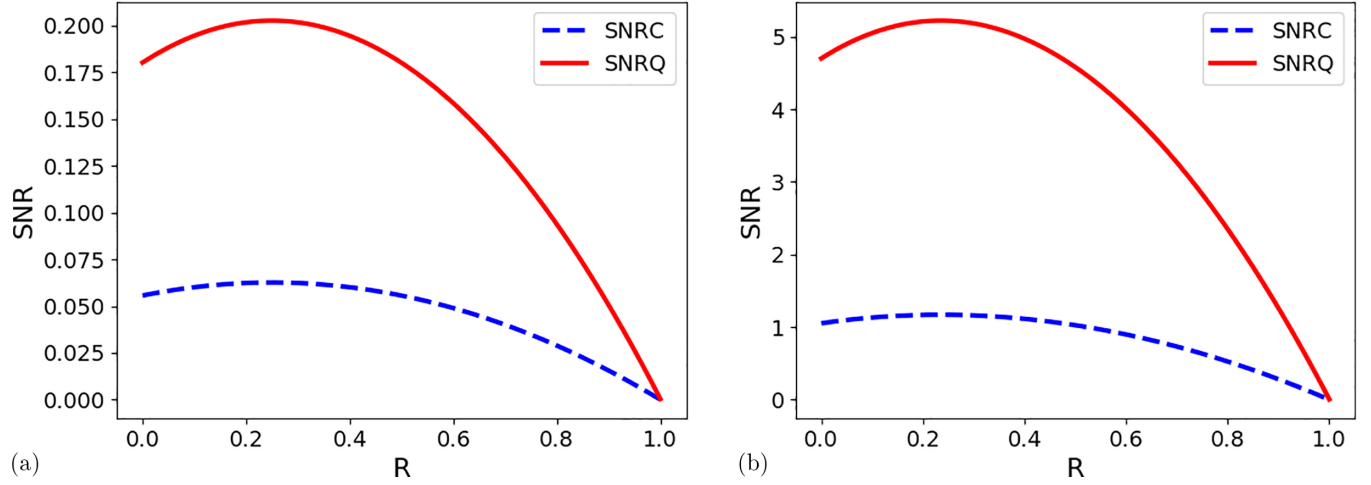


FIG. 7. The SNRs for both the conventionally acquired image and IFQI image as a function of the BS reflectivity,  $R$ , are plotted for (a)  $\bar{N} = 0.5$  and (b)  $\bar{N} = 10$ . The blue dashed line corresponds to the theoretical prediction for conventionally acquired images and the red solid line corresponds to the theoretical prediction of using the AND operation. The SNRs are determined with  $d = 10$ ,  $\mathcal{T} = 10$ ,  $\eta = 0.001$ , and  $\epsilon = 0.001$ .

visibility of IFQI ( $V_Q$ ), which is obtained from correlated photons using the AND operation, and the visibility of the conventional image ( $V_C$ ),

$$A = \frac{V_Q}{V_C}. \quad (30)$$

Visibility, as defined in Eq. (25), is the ratio between the difference of the bright region and the dark region intensities of the final summed image and the sum of these intensities. If an average of  $\bar{N}$  photons enter each signal and the reference arm from the SPDC process, then we can write the photon number that is detected in the bright and the dark parts of the object of the conventionally acquired image for the idler exit ports:  $N_{B,D_2(\epsilon \neq 0)}^C = \bar{N}R^2 + \epsilon\bar{N}T^2 + \mathcal{T} + d$  and  $N_{D,D_2(\epsilon=0)}^C = \bar{N}R^2 + \mathcal{T} + d$ . Also, these numbers of photons at detector  $D_1$  are  $N_{B,D_1(\epsilon \neq 0)}^C = \bar{N}RT + \epsilon\bar{N}RT + \mathcal{T} + d$  and  $N_{D,D_1(\epsilon=0)}^C = \bar{N}RT + \mathcal{T} + d$ . Now by subtracting the bright regions' intensities of  $D_1$  and  $D_2$ ,  $N_{B,D_1(\epsilon \neq 0)}^C$  and  $N_{B,D_2(\epsilon \neq 0)}^C$ ,

from each other, and by subtracting the dark regions  $N_{D,D_1(\epsilon=0)}^C$  and  $N_{D,D_2(\epsilon=0)}^C$ , we can rewrite visibility of the conventionally acquired image as follows:

$$\begin{aligned} V_C &= \frac{|\Delta N_{B,D_1,D_2}^C - \Delta N_{D,D_1,D_2}^C|}{\Delta N_{B,D_1,D_2}^C + \Delta N_{D,D_1,D_2}^C} \\ &= \frac{|(N_{B,D_1(\epsilon \neq 0)}^C - N_{B,D_2(\epsilon \neq 0)}^C)| - |(N_{D,D_1(\epsilon=0)}^C - N_{D,D_2(\epsilon=0)}^C)|}{|(N_{B,D_1(\epsilon \neq 0)}^C - N_{B,D_2(\epsilon \neq 0)}^C)| + |(N_{D,D_1(\epsilon=0)}^C - N_{D,D_2(\epsilon=0)}^C)|}. \end{aligned} \quad (31)$$

One can then write the photon number that is detected in the bright and dark parts of the object IFQI image for the idler exit port:  $N_{B,D_2(\epsilon \neq 0)}^Q = (R^2 + \epsilon T^2)\eta\bar{N} + \{\bar{N}[1 - (R^2 + \epsilon T^2)\eta] + d\}[\bar{N}(R^2 + \epsilon T^2)(1 - \eta) + \mathcal{T} + d]$  and  $N_{D,D_2(\epsilon=0)}^Q = \eta\bar{N}R^2 + [\bar{N}(1 - R^2\eta) + d][\bar{N}R^2(1 - \eta) + \mathcal{T} + d]$ . Thus, for detector  $D_1$ , we have  $N_{B,D_1(\epsilon \neq 0)}^Q = (RT + \epsilon RT)\eta\bar{N} + \{\bar{N}[1 - (RT + \epsilon RT)\eta] + d\}[\bar{N}(RT + \epsilon RT)(1 - \eta) + \mathcal{T} + d]$

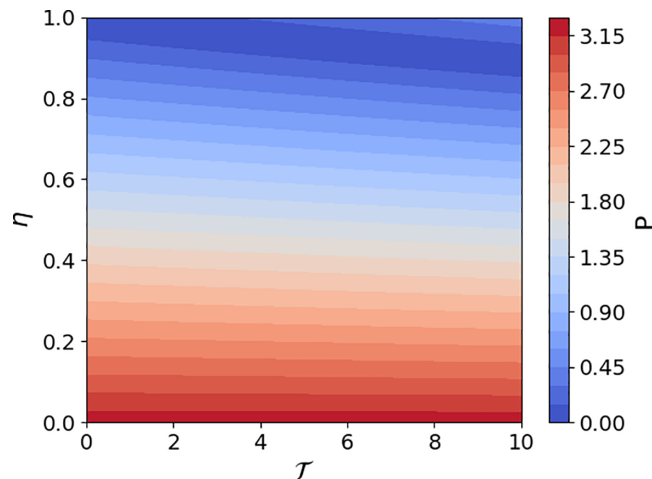


FIG. 8. The power as a function of  $\eta$  and  $\mathcal{T}$  (plotted for  $\bar{N} = 0.5$ ,  $d = 10$ ,  $\epsilon = 0.001$ , and  $R = 0.24$ ).

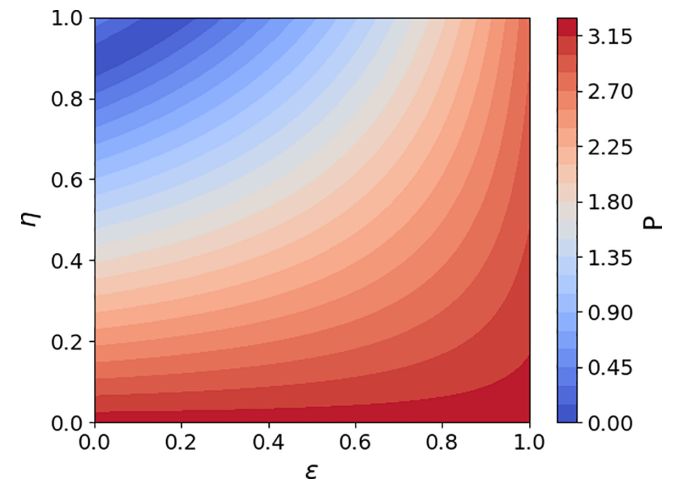


FIG. 9. The power as a function of  $\epsilon$  and  $\eta$  (plotted for  $\bar{N} = 0.5$ ,  $d = 10$ ,  $\mathcal{T} = 10$ , and  $R = 0.24$ ).



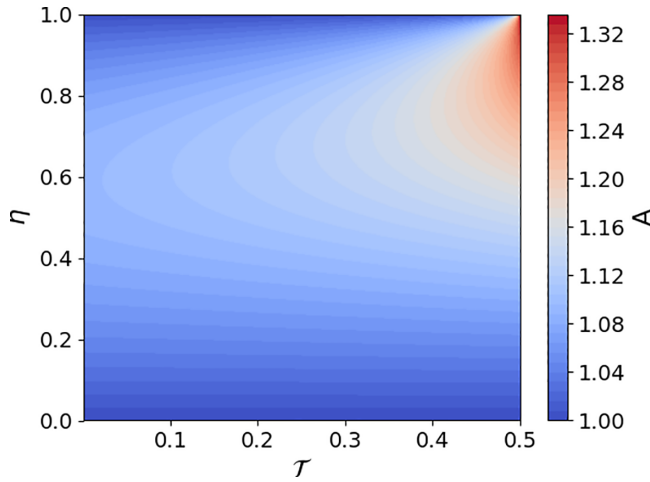


FIG. 10. The advantage is obtained as a function of  $\eta$  and  $\mathcal{T}$  (plotted for  $\bar{N} = 0.5$ ,  $d = 0.5$ ,  $\epsilon = 0.001$ , and  $R = 0.5$ ).

and  $N_{D,D_1(\epsilon=0)}^Q = \eta\bar{N}RT + [\bar{N}(1 - RT\eta) + d][\bar{N}RT(1 - \eta) + \mathcal{T} + d]$ . Like the conventionally acquired image, the visibility of the IFQI AND image is given by

$$V_Q = \frac{|\Delta N_{B,D_1,D_2}^Q - \Delta N_{D,D_1,D_2}^Q|}{\Delta N_{B,D_1,D_2}^Q + \Delta N_{D,D_1,D_2}^Q} = \frac{|(N_{B,D_1(\epsilon \neq 0)}^Q - N_{B,D_2(\epsilon \neq 0)}^Q) - |(N_{D,D_1(\epsilon=0)}^Q - N_{D,D_2(\epsilon=0)}^Q)|}{|(N_{B,D_1(\epsilon \neq 0)}^Q - N_{B,D_2(\epsilon \neq 0)}^Q)| + |(N_{D,D_1(\epsilon=0)}^Q - N_{D,D_2(\epsilon=0)}^Q)|}. \quad (32)$$

We are now in a position to calculate the IFQI advantage from Eq. (30).

As the advantage  $A$  is a function of experimental parameters, we have plotted it as a function of  $\eta$  and  $\mathcal{T}$  in Fig. 10, and as a function of  $\epsilon$  and  $\eta$  in Fig. 11. We found that the advantage increases with increasing both  $\eta$  and  $\mathcal{T}$ . It means that the uncorrelated background in the IFQI image can be rejected more than a conventionally acquired image.

In Fig. 11, we can see the advantage  $A$  as a function of  $\epsilon$  and  $\eta$ . As shown in this figure, the advantage decreases with

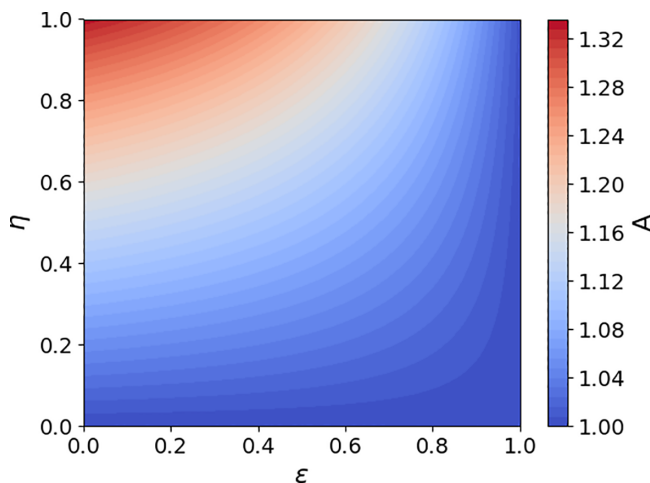


FIG. 11. The advantage is obtained as a function of  $\eta$  and  $\epsilon$  (plotted for  $\bar{N} = 0.5$ ,  $d = 0.5$ ,  $\mathcal{T} = 0.5$ , and  $R = 0.5$ ).

increasing  $\epsilon$ . So, we can understand that the AND operation will perform better, especially for a low-reflectivity object. In addition, this improvement will increase by decreasing environmental noise, i.e., increasing  $\eta$ . Since the main focus is on the low-reflectivity objects, IFQI leads us to our main goal.

#### IV. SUMMARY

In this research, we were interested to see whether a new quantum optical method is possible for imaging with fewer photons than conventional imaging techniques, but with better visibility and resolution even if the detected photons did not previously interact with the object. In fact, sometimes a target is in a situation where an unwanted background is generated in the image. Here, we have presented an interaction-free quantum imaging (IFQI) protocol to achieve a resolution enhancement and background rejection through the AND operation in the presence of both background light and noise. The suggested IFQI protocol is a technique for quantum imaging that has not been tested before. We have analytically derived and numerically validated the basic parameters in imaging methods such as SNR and visibility, and have shown the benefits of this method by introducing two quantities, power and advantage.

Our IFQI method combines two different techniques: interaction-free ghost imaging (IFGI) and correlation-based quantum imaging (CBQI); but with better efficiency, which has advantages over the two techniques separately. Perhaps IFQI can somehow be an upgrade of the IFGI protocol; however, with some significant differences. In the IFGI, there is no thermal radiation in the setup and the effect of noise is not considered, while IFQI considers the effects of noise. In the IFQI method, there is an additional entangled beam as a reference beam (i.e., it looks like we have two idler beams) than one idler beam in IFGI. Moreover, IFQI uses the AND protocol to remove the background and thermal noise efficiently, while IFGI does not. Our setup reaches higher transparency than IFGI. Additionally, we have shown in this paper how an interferometer enhances detection efficiency.

Table I shows a comparison of the four imaging methods for SNR and visibility, and Table II indicates the benefits of the IFQI method under different number of incident photons. However, in order to prove the real advantages of the technique, it should be tested experimentally, which may find application in the imaging of photosensitive biological tissues in a noninvasive and harm-free fashion.

Regarding the structured objects, in the IFGI part of the setup, the interference between the two paths provides information about the presence or absence of objects along the path of the photon that passes through the object. By repeating this process many times, a statistical image of the object can be built up, allowing its structure to be determined [10]. This method is referred to as “interaction free” because the object is not physically disturbed; only its presence or absence is determined. Moreover, the object’s spatial properties can be reconstructed by collecting data from different angles and using methods such as tomography [24], which can collect data from different angles and use mathematical algorithms to reconstruct an image of the object. The mathematical

TABLE I. SNR and visibility of four imaging methods for three different input photon numbers. We assumed  $R = 0.23$ ,  $d = 10.0$ ,  $\mathcal{T} = 10.0$ ,  $\eta = 0.001$ ,  $\epsilon = 0.001$ . Comparisons are between four methods: conventional, correlation-based quantum imaging (CBQI), interaction-free ghost imaging (IFGI), and interaction-free quantum imaging (IFQI).

	Photons/pixel	Conventional	CBQI	IFGI	IFQI
SNR	$N = 0.5$	0.07848836	0.02234949	0.06258121	0.20255484
	$N = 1.0$	0.15601568	0.03160696	0.12468741	0.41306164
	$N = 10.0$	1.41265809	0.09994998	1.16967163	5.22410194
Visibility	$N = 0.5$	0.00001249	0.00050025	0.00167671	0.00167673
	$N = 1.0$	0.00002499	0.00050025	0.00167671	0.00167675
	$N = 10.0$	0.00024993	0.00050025	0.00167671	0.00167691

algorithms can be iterative reconstruction techniques [25,26], a filtered back-projection algorithm [27], the algebraic reconstruction technique (ART) [24], or multiplexed measurements [28].

### ACKNOWLEDGMENTS

V.S. acknowledges the support of the Alberta Innovates grant. S.B. acknowledges funding by the Natural Sciences and Engineering Research Council of Canada (NSERC) through

its Discovery Grant, funding and advisory support provided by Alberta Innovates through the Accelerating Innovations into CarE (AICE) Concepts Program, and support from Alberta Innovates and NSERC through Advance Grant. This project is funded [in part] by the Government of Canada. Ce projet est financé [en partie] par le gouvernement du Canada. All authors wish to acknowledge the fruitful discussions with Ebrahim Karimi and Dilip Paneru for reading the first draft of the manuscript and giving us helpful comments to improve the paper.

TABLE II. Power and advantage of our interaction-free quantum imaging (IFQI) method against three other imaging methods: conventional, correlation-based quantum imaging (CBQI), and interaction-free ghost imaging (IFGI). We assumed  $R = 0.23$ ,  $d = 10.0$ ,  $\mathcal{T} = 10.0$ ,  $\eta = 0.001$ ,  $\epsilon = 0.001$ .

	Photons/pixel	IFQI/conventional	IFQI/CBQI	IFQI/IFGI
Power	$N = 0.5$	2.58069895	9.06306092	3.23667196
	$N = 1.0$	2.64756481	13.06869195	3.31277720
	$N = 10.0$	3.69806535	52.26715953	4.46629789
Advantage	$N = 0.5$	134.14072419	3.35179945	1.00001095
	$N = 1.0$	67.07186826	3.35183282	1.00002091
	$N = 10.0$	6.70932663	3.35214795	1.00011492

- [1] G. B. Lemos, V. Borish, G. D. Cole, S. Ramelow, R. Lapkiewicz, and A. Zeilinger, Quantum imaging with undetected photons, *Nature (London)* **512**, 409 (2014).
- [2] P. Kwiat, H. Weinfurter, T. Herzog, A. Zeilinger, and M. A. Kasevich, Interaction-Free Measurement, *Phys. Rev. Lett.* **74**, 4763 (1995).
- [3] A. G. White, J. R. Mitchell, O. Nairz, and P. G. Kwiat, Interaction-free imaging, *Phys. Rev. A* **58**, 605 (1998).
- [4] A. Gatti, E. Brambilla, M. Bache, and L. A. Lugiato, Correlated imaging, quantum and classical, *Phys. Rev. A* **70**, 013802 (2004).
- [5] T. Gregory, P.-A. Moreau, E. Toninelli, and M. J. Padgett, Imaging through noise with quantum illumination, *Sci. Adv.* **6**, eaay2652 (2020).
- [6] P.-A. Moreau, E. Toninelli, T. Gregory, and M. J. Padgett, Imaging with quantum states of light, *Nat. Rev. Phys.* **1**, 367 (2019).
- [7] A. M. Palici, T. A. Isdraila, S. Ataman, and R. Ionicioiu, Interaction-free imaging of multipixel objects, *Phys. Rev. A* **105**, 013529 (2022).
- [8] Y. Yang, H. Liang, X. Xu, L. Zhang, S. Zhu, and X.-S. Ma, Interaction-free, single-pixel quantum imaging with undetected photons, *npj Quantum Inf.* **9**, 2 (2023).
- [9] P. Ben Dixon, Quantum ghost imaging through turbulence, *Phys. Rev. A* **83**, 051803(R) (2011).
- [10] Y. Zhang, A. Sit, F. Bouchard, H. Larocque, F. Grenapin, E. Cohen, A. C. Elitzur, J. L. Harden, R. W. Boyd, and E. Karimi, Interaction-free ghost-imaging of structured objects, *Opt. Express* **27**, 2212 (2019).
- [11] V. Salari, Quantum face recognition protocol with ghost imaging, *Sci. Rep.* **13**, 2401(2023).
- [12] J. H. Shapiro, The quantum illumination story, *IEEE Aerosp. Electron. Syst. Mag.* **35**, 8 (2020).
- [13] S. Barzanjeh, S. Pirandola, D. Vitali, and J. M. Fink, Microwave quantum illumination using a digital receiver, *Sci. Adv.* **6**, eabb0451 (2020).
- [14] S. Barzanjeh, S. Guha, C. Weedbrook, D. Vitali, J. H. Shapiro, and S. Pirandola, Microwave Quantum Illumination, *Phys. Rev. Lett.* **114**, 080503 (2015).

- [15] E. D. Lopaeva, I. Ruo Berchera, I. P. Degiovanni, S. Olivares, G. Brida, and M. Genovese, Experimental Realization of Quantum Illumination, *Phys. Rev. Lett.* **110**, 153603 (2013).
- [16] P.-A. Moreau, E. Toninelli, T. Gregory, and M. J. Padgett, Ghost imaging using optical correlations, *Laser Photon. Rev.* **12**, 1700143 (2018).
- [17] M. Genovese, Real applications of quantum imaging, *J. Opt.* **18**, 073002 (2016).
- [18] J. Schneeloch, S. H. Knarr, D. F. Bogorin, M. L. Levangie, C. C. Tison, R. Frank, G. A. Howland, M. L. Fanto, and P. M. Alsing, Introduction to the absolute brightness and number statistics in spontaneous parametric down-conversion, *J. Opt.* **21**, 043501 (2019).
- [19] C. Zhang, Y.-F. Huang, B.-H. Liu, C.-F. Li, and G.-C. Guo, Spontaneous parametric down-conversion sources for multiphoton experiments, *Adv. Quantum Technol.* **4**, 2000132 (2021).
- [20] I. Ruo-Berchera, Theory of PDC in a continuous variables framework and its applications to the absolute calibration of photo-detectors, *Adv. Sci. Lett.* **2**, 407 (2009).
- [21] G. Brida, M. V. Chekhova, G. A. Fornaro, M. Genovese, E. D. Lopaeva, and I. R. Berchera, Systematic analysis of signal-to-noise ratio in bipartite ghost imaging with classical and quantum light, *Phys. Rev. A* **83**, 063807 (2011).
- [22] E. Brambilla, A. Gatti, M. Bache, and L. A. Lugiato, Simultaneous near-field and far-field spatial quantum correlations in the high-gain regime of parametric down-conversion, *Phys. Rev. A* **69**, 023802 (2004).
- [23] A. Gatti, E. Brambilla, and L. A. Lugiato, Correlated imaging with entangled light beams, in *Quantum Communications and Quantum Imaging*, Vol. 5161 (SPIE, 2004) pp. 192–203.
- [24] G. T. Herman, *Fundamentals of Computerized Tomography: Image Reconstruction from Projections*, 2nd ed. (Springer, Dordrecht, 2009).
- [25] J. A. Fessler, Penalized weighted least-squares image reconstruction for positron emission tomography, *IEEE Trans. Med. Imaging* **13**, 290 (1994).
- [26] W. Wang, Y. P. Wang, J. Li, X. Yang, and Y. Wu, Iterative ghost imaging, *Opt. Lett.* **39**, 5150 (2014).
- [27] T. Wuerfl, M. Hoffmann, V. Christlein, K. Breininger, Y. Huang, M. Unberath, and A. Maier, Deep learning computed tomography: Learning projection-domain weights from image domain in limited angle problems, *IEEE Trans. Med. Imaging* **37**, 1454 (2018).
- [28] K. Heinzmann, L. M. Carter, J. S. Lewis, and E. O. Aboagye, Multiplexed imaging for diagnosis and therapy, *Nat. Biomed. Eng.* **1**, 697 (2017).